Modeling and Analysis

GREENHOUSE GASES SCIENCE AND TECHNOLOGY

Prediction of supercritical CO_2/brine relative permeability in sedimentary basins during carbon dioxide sequestration

Afshin Tatar, **Amin Shokrollahi**, Young Researchers and Elite Club, North Tehran Branch, Islamic Azad University, Tehran, Iran
Moonyong Lee, School of Chemical Engineering, Yeungnam University, Gyeungsan, Republic of Korea
Tomoaki Kashiwao, Department of Electronics and Control Engineering, National Institute of Technology, Niihama, Japan
Alireza Bahadori, Southern Cross University, School of Environment, Science and Engineering, Lismore, NSW, Australia

Abstract: This study aims to accurately determine supercritical CO_2/brine relative permeability, using a hybrid Genetic Algorithm-Radial Basis Function (GA-RBF) neural network. CO_2 sequestration, along with some enhanced oil recovery (EOR) processes, demands an exact knowledge of relative permeability in order to ensure the viability of the operation. Previous studies have shown that errors in CO_2/brine relative permeability data might result in a four-fold error in injectivity estimation. This, as well as several recent studies regarding the relative permeability of CO_2/brine systems, has indicated the importance of this parameter. The developed GA-RBF model was determined to be in excellent accordance with experimental data, yielding average absolute relative deviations (AARD) of 4.66% and 2.11% for CO_2 and brine relative permeability, respectively. In addition, comprehensive comparisons between classic models and the proposed GA-RBF model have been carried out. Based on these comparisons, it may be concluded that the proposed model is superior to the classic method (simple correlation) in terms of its accuracy in determining the viability of CO_2 sequestration operations.

Keywords: supercritical CO_2 relative permeability; brine relative permeability; artificial intelligence; radial basis function (RBF); classic correlations; CO_2 sequestration

Introduction

Global warming, occurring due to the anthropogenic release of greenhouse gases (GHGs), is now a serious concern worldwide.[1] A large amount of CO_2 is emitted from large stationary sources, such as refineries, power plants, and fertilizer plants. For example, a large coal-fired power plant emits about 8 million tons of CO_2 in a year.[2] Our dependency on fossil fuels is expected to continue throughout this century[3,4] Carbon dioxide capture and sequestration (CCS) to deep underground formations

Correspondence to: Amin Shokrollahi, Young Researchers and Elite Club, North Tehran Branch, Islamic Azad University, Tehran, Iran. E-mail: shokrollahi.amin@gmail.com; Alireza Bahadori, Southern Cross University, School of Environment, Science and Engineering, Lismore, NSW, Australia. E-mail: alireza.bahadori@scu.edu.au
Received July 17, 2014; revised April 30, 2015; accepted June 29, 2015
Published online at Wiley Online Library (wileyonlinelibrary.com). DOI: 10.1002/ghg.1524

is an effective way to reduce emissions of GHGs to the atmosphere.

Depleted oil and gas reservoirs, saline aquifers, and coal beds are potential candidates for CO_2 sequestration. Depleted oil and gas reservoirs, saline aquifers, and unmineable coal beds have respective capacities of 675–900 Gt, 1000–10 000 Gt, and 3–200 Gt of CO_2 for sequestration.[5] However, despite there being some progresses in our estimation of capacity, as well as an improvement in regional estimations, the estimates for saline aquifers and coal beds retain a large degree of uncertainty.[6] While the current technology which is applied to CO_2 sequestration in coal beds is relatively immature, it is known that these structures are not as common as aquifers.[7]

CO_2 sequestration in oil fields for the purposes of enhanced oil recovery (EOR) might be the best choice. However, this is only economically feasible in fields where sequestration costs can be offset by the additional oil yield. Sequestration in depleted oil and gas reservoirs is an attractive option due to the existence of detailed knowledge of their physical structures, as well as the potential pre-existence of facilities onsite. Nevertheless, this choice associates with geographical limitations.

Some abandoned wells might be brought back into production in future years, due to the potential for oil and gas prices to increase. Deep saline aquifers are widespread, and tend to have larger capacities than the other candidates mentioned. Ocean basins may seem like ideal candidates for CO_2 sequestration, however, there are a number of problems associated with their utilization, such as poor knowledge of their structural characteristics and chemical processes, high costs, technical limitations, environmental considerations, and physical barriers to efficient sequestration.[8]

It is expected that the deep injection of CO_2 to aquifers will increase significantly in the first half of the current century due to the great capacity of these aquifers.[9] The technology for fluid injection deep into the earth is relatively well-developed, as it is currently utilized by industries for EOR purposes, as well as for the deep injection of other liquid wastes,[10] as well as for the disposal of acid gas.[11]

The physical state of CO_2 depends on the pressure and temperature at which it is held.[12] Under ambient conditions, CO_2 occurs in the gaseous state, but becomes liquid when stored under high temperature/pressure deep underground. CO_2 injected into underground formations turns into supercritical fluid due to the high temperatures it encounters. In cases where CO_2 is injected into oil and gas reservoirs and saline aquifers, the *in situ* fluid is more dense than CO_2, and thus, the CO_2 rises to the base of the caprock.[2]

To be more specific, at a depth of about 600–1000 m, CO_2 is present in the supercritical phase (i.e., it behaves like a gas, but has the density of a liquid).[13] For lower depths, depending on the temperature and pressure, CO_2 may occur in gaseous or liquid states. Generally speaking, CO_2 should be injected to depths at which it will remain at a relatively high density (either as a liquid or in the supercritical phase), so that the utilization of the pore space is optimal.[5] However, in some cases it may be economically feasible to store CO_2 in the gaseous state.

Several mechanisms can be utilized for CO_2 sequestration below caprock in oil and gas reservoirs, such as static or hydrodynamic trapping. In deep saline aquifers, *in situ* mineral carbonation, dissolution in reservoir oil or formation water, adsorption onto organic matter in coal and shale, and CO_2 retention as an immobile phase trapped in the pore space of deep saline aquifers have been proposed.[14,15]

As has been mentioned, CO_2 rises to reach the base of the caprock. Due to diffusion-limited mass transfer, centuries or millennia may be necessary for CO_2 to dissolve into formation water, allowing for its reaction with available minerals.[16,17]

Relative permeability is a parameter that influences CO_2 injection, migration, and storage processes.[18] In addition, in CO_2-EOR projects, injected CO_2 will come into contact with formation water. The final distribution of CO_2 underground is highly effected by relative permeability.[19–21] It should be noted that models and simulations which aim to accurately predict the behavior of the CO_2-brine systems require these data.[22]

Burton *et al.*[23] determined that uncertainty in relative permeability data might result in up to a four-fold variation in the overall estimation of injection capacity. Several additional recent studies regarding this parameter[24–32] have indicated its importance.

The most critical parameters which effect CO_2-brine relative permeability are pressure, temperature, and salinity.[33] In addition, higher IFT values lead to greater non-linearity between fluid saturation and relative permeability.[18]

While a wealth of data exists for CO_2-oil systems, few measurements are available for CO_2-brine systems,[8,34]

as CO_2 sequestration in geological structures, especially in deep aquifers, is an emerging technology.

As an example of this, no relevant data for the relative permeability of CO_2-brine systems have been made available prior to 2005.[35] Reservoir parameters are available for petroleum industrial regions due to previous studies of the oil fields, but CO_2-brine relative permeability[33] remains a time-consuming and expensive process which, contrary to data from oil and mineral exploration, is not available as a by-product of an additional industry.[36]

The aim of this study was to determine supercritical CO_2/brine relative permeability using an intelligent system. In this study, a radial basis function neural network was utilized due to its great flexibility and capability in the recognition of complex patterns.[37–40] To the best of our knowledge, a radial basis function neural network has not previously been used to predict CO_2/brine relative permeability. In addition, the proposed network has been compared with two classic correlations.

Details of intelligent model

Artificial neural networks (ANNs) are capable of learning from experience, improving their performance, and adapting to the changes in the environment.[41] The main advantages of neural networks lie in their ability to process a large amount of data, and their ability to generalize the results arising from this data. ANNs are parallel distributed systems that are composed of artificial neurons as processing units. These units are arranged in layer(s), which are interconnected.

Multi-layer perceptron (MLP) networks and radial basis function (RBF) are two of the most popular ANNs in existence today. These two networks have the same applications but different internal calculation structures. The greatest advantage of RBFNs is their simple design, having just three layers. They are capable of good generalization, have high tolerance to input noises, and have a capability for online learning.[41] In terms of generalization, RBFNs can respond very well to patterns which have not been encountered during training.[42]

The RBFN is a universal approximator, having a solid foundation in conventional approximation theory.[43] RBF has a simpler structure than MLP, and the training process requires much less time due to its relatively simple structure. These features make RBF a popular alternative to MLP. The origin of RBF is in performing exact interpolations of sets of data points in a multidimensional space.[44] It has been proven that RBF networks can carry out a similar function to that of MLP networks, but with increased input dimensions.[45] The architecture of RBF resembles a classic regularization network,[46] which may be said to hold three generally accepted desirable properties.[46,47]

1. It is capable of approximating any multivariate continuous function on a compact domain, and to a specified accuracy, given sufficient data.
2. The solution is optimal in the sense that it is capable of determining a function, which represents the lowest degree of variation.
3. The approximation has the best-approximation property since unknown coefficients are assumed to be linear.

The architecture of an RBF is somewhat similar to that of MLP (Fig. 1). It has three layers: the input layer, the hidden layer, and the output layer. As a non-linear activation function, each node in the hidden layer uses an RBF ($\phi(r)$). The input layer is composed of an input vector which undergoes a non-linear transformation in the hidden layer. In other words, the hidden layer consists of an RBF activation function as network neuron.

The net input to the RBF activation function is the vector distance between its weight and the input vector that is multiplied by the corresponding bias. The output layer is a linear combiner, which maps the non-linearity into a new space. It is possible to model the biases of the output layer neurons using an additional neuron in the hidden layer, which possess a constant activation function $\phi_0(r)=1$. An RBFN can achieve a global optimal solution to the adjustable weights in the minimum MSE sense, using the linear optimization method.[43] However, there are a number of fundamental differences between RBF and MLP networks, the most important of which are listed below.[42]

1. RBF networks are relatively simple compared to MLP networks.
2. Due to their simple and fixed three-layer architecture, RBFNs are easier to train than MLP networks.
3. RBF networks act as local approximation networks and the network outputs are determined by specified hidden units in certain local receptive fields, while MLP networks work globally, with network outputs being decided by all neurons.

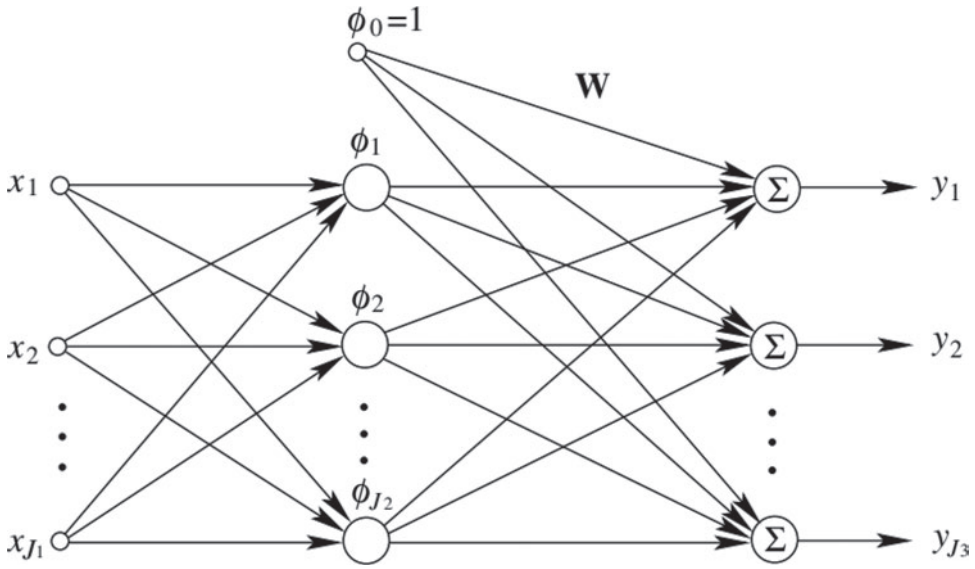

Figure 1. Schematic representation of RBFN.[43]

4. The classification methods which are used in RBF and MLP networks are quite different. RBF networks clusters are separated by hyper spheres, while MLP network clusters are separated by hyper surfaces.

For an input pattern x, the output of the network is given by:

$$y_i(x)=\sum_{k=1}^{J_2} w_{ki}\phi(\ \|x-c_k\|\ ) \tag{1}$$

For $i=1,...,J_3$, where $y_i(x)$ is the i^{th} output of the RBF, w_{ki} is the connection weight from the k^{th} hidden unit to the i^{th} output unit, c_k is prototype of center of the k^{th} hidden unit, and $\|\cdot\|$ denotes the Euclidean norm. The RBF $\phi(.)$ is typically selected as the Gaussian function.[43]

For a set of N pattern pairs of $\{(x_p, y_p)\}$, Eqn (1) can be expressed in matrix form:

$$Y=W^T\Phi \tag{2}$$

Where $W=[w_1,...,w_{J_3}]$ is a $J_2\times J_3$ is weight matrix in which $w_i=(\omega_{1i},...,\omega_{J_2 i})^T$, $\Phi=[\phi_1,...,\phi_N]^T$ is a $J_2\times N$ matrix, $\phi_p=(\phi_{p,1},...,\phi_{p,J_2})^T$ is the output of the hidden layer for the p^{th} sample, $\phi_{p,k}=\phi(\ \|x_p-c_k\|\ )$, $Y=[y_1 y_2 y_N]$ is a $J_3\times N$ matrix, and $y_p=(y_{p,1},...,y_{p,J_3})^T$.

If RBF is suitably applied, it can theoretically approximate any continuous function arbitrarily well.[46,48,49] RBFs have good mathematical properties. In the context of the exact interpolation problem, many properties of the interpolating function are relatively insensitive to the precise form of the nonlinear function $\phi(.)$.[44]

The Gaussian RBFN can approximate any continuous function by a sufficient number of centers $c_i, i=1,...,J_2$, and a common standard deviation $\sigma>0$ in the L_p -norm, $p\in[1,\infty]$.[50] It is possible that a class of RBFNs achieve universal approximation when the RBF is continuous and integrable.[50]

The learning of RBFN is formulated as the minimization of the MSE function, just as in the case of MLP:

$$E=\frac{1}{N}\sum_{i=1}^{N}\ \|y_p-W^T\phi_p\|^2=\frac{1}{N}\ \|Y-W^T\Phi\|_F^2 \tag{3}$$

where $Y=[y_1,y_2,...,y_N]$, y_i is the target output for the i^{th} sample in the training set, and $\|\cdot\|_F$ is the Frobenius norm, defined as $\|A\|_F^2=tr(A^TA)$. For learning of RBFN, it is necessary to determine the RBF centers and the corresponding weights. The selection of the RBF centers is the most important point in the suitable implementation of RBFN. The possible centers may be placed on a random subset, or can be determined via either clustering or a learning procedure. It is also possible to initially choose all the data points as the centers and then remove some of them through a selective use of the k-NN classification scheme. [51]

The value of radial functions increases or decreases in relation to the distance from a central point.

Among the several types of radial basis functions, the most commonly used is the Gaussian function, Eqn (4).[42] Some of the functions that can be used as the RBF are as follows.[46,48,52]

$$\phi(r)=e^{-\frac{r^2}{2\sigma^2}}, \qquad Gaussian \tag{4}$$

$$\phi(r)=\frac{1}{\left(\sigma^2+r^2\right)^{\alpha}}, \qquad \alpha>0 \tag{5}$$

$$\phi(r)=\left(\sigma^2+r^2\right)^{\beta}, \qquad 0<\beta<1 \tag{6}$$

$$\phi(r)=r, \qquad linear \tag{7}$$

$$\phi(r)=r^2\ln(r) \qquad thin-platespline \tag{8}$$

$$\phi(r)=r^3, \qquad cubic \tag{9}$$

$$\phi(r)=\frac{1}{1+e^{\frac{r}{\sigma}-\theta}}, \qquad logistic\ function \tag{10}$$

where $r>0$ represents the distance from a data point, x, to a center, c, while σ in Eqns (4) through (6) and in Eqn (10), is a parameter that controls the smoothness of the interpolating function, and θ in Eqn (10) is adjustable bias. In this study, Gaussian radial function is used due to its large degree of flexibility.

Result and discussion

Data acquisition

The success of model development based on machine learning methods significantly depends on the accuracy of the experimental measurements. Upon reviewing previous studies regarding CO_2/brine relative permeability, it can be concluded that this factor is a function of porosity, absolute permeability, interfacial tension (IFT), pore pressure, temperature, capillary pressure, brine's salinity, rock type, and phase saturation.[6,9,11,13,18,35,53,54]

Data used in this study have been gathered from open literature.[34,53,54] These data were acquired from supercritical CO_2/brine relative permeability tests on different sandstone and carbonate formations. All the experiments were performed under simulated reservoir conditions. Reservoir and fluid characteristics are listed in Table 1. Details of the experimental procedure and conditions have been previously published.[34,53,54] The statistical parameters of the data are presented in Table 2.

Model development

The dataset was initially divided into training and testing datasets, accounting for 80% and 20% of the total data set, respectively. Data point allocation should be such that there is no local accumulation for training or testing datasets.

RBF neural networks were utilized for this study. In Matlab® implementation, this network has two tuning parameters, namely, the Spread and Maximum Number of Neurons. The optimum values of mentioned parameter results in the best performance of the network. A genetic algorithm was utilized to determine the optimum values. In this respect, 100 random solutions were generated as the initial population. The fitness of each solution was then evaluated and the population was sorted based on this outcome. The GA operators (crossover and mutation) were then applied to determine the next generation.

Stopping criteria was the maximum allowable number of generation. After 40 generations, the optimum values for Spread and Maximum Number of Neurons, respectively, were determined to be 1.28 and 165 for CO_2 and 0.5156 and 119 for brine relative permeability. The convergence of genetic algorithm to the optimum values is illustrated in Figs 2 and 3 for CO_2 and brine relative permeability, respectively.

Accuracy of the proposed model and validation

In order to assess the accuracy and validity of the proposed model, both graphical and statistical methods were utilized. First of all, the GA-RBF model's outputs were compared with the experimental data. They were then compared with two well-known correlations in order to determine the relative permeability, namely Corey[55] and by power laws.[56]

Two types of plots, namely cross-plot and error deviation, were utilized to investigate the accuracy of the proposed GA-RBF model. Cross-plots corresponding with CO_2 and brine relative permeability are presented in Figs 4 and 5, respectively. It can be clearly observed that all the data points are concentrated in close vicinity to the 45° line. This shows the superiority of the proposed model, as

Table 1. Rock and fluid characteristics gathered from literature.[34, 53, 54]

	Area	Porosity (%)	Permeability (mD)	IFT (mN/m)	Salinity (mg/L)	Pressure (MPa)	Threshold Capillary pressure (kPa)	Temperature (°C)	Rock Type
Krevor *et al*.[34]	Area #1	22.1	914	32	50	9	2.5	50	sandstone
	Area #2	28.3	1156	32	50	9	2.1	50	sandstone
	Area #3	24.4	7.5	32	50	9	4.6	50	sandstone
Bennion and Bachu[53]	Area #4	12.5	2.7	32.1	28300	8.6	28.8	35	sandstone
	Area #5	19.5	21.72	32.1	28300	8.6	3.5	35	sandstone
	Area #6	12.6	0.376	32.5	97200	10.9	56.3	40	sandstone
	Area #7	11.7	0.081	27	248000	27	31.9	75	sandstone
Bennion and Bachu[54]	Area #8	10.9	74.4	34.6	136800	17.4	28.2	56	carbonate
	Area #9	11.8	153.9	29.5	144300	11.9	14.5	41	carbonate
	Area #10	11.6	371.9	33.1	103701	11.4	14.5	40	carbonate
	Area #11	16.8	353.6	35.1	106069	9.2	21.3	36	carbonate
	Area #12	16.7	4.87	35.7	233400	15.5	69	55	carbonate
	Area #13	9.9	0.217	29.5	129145	18.8	802	43	carbonate
	Area #14	14.8	3.09	45.3	320847	8.73	55	36	carbonate

predicted values are in close agreement with experimental data.

To assess the deviation of predicted values from experimentally measured data, relative deviation has been plotted for CO_2 and brine relative permeability in Figs 6 and 7, respectively.

In order to provide for a better comparison between GA-RBF predicted and real values, these have been plotted against an index of data points in Figs 8 and 9 for CO_2 and brine relative permeability, respectively.

Four different parameters – correlation factor (R^2), Average Absolute Relative Deviation (AARD), Stan-

Table 2. Statistical parameters of input and output values

Input Parameter	Minimum	Maximum	Average	Standard Deviation
Porosity (%)	9.9	28.3	14.319	4.360
Permeability (mD)	0.081	1156	148.123	259.940
IFT (mN/m)	27	45.3	33.262	4.312
Salinity (mg/L)	50	320847	132645.200	89646.710
Pressure (MPa)	8.6	27	13.269	5.234
Threshold Capillary Pressure (kPa)	2.1	802	91.754	212.741
Temperature (°C)	35	75	45.713	11.125
Rock Type	1	2	1.632	0.483
Sg	0	0.7892	0.247	0.179
Sw	0.2108	1	0.752	0.180
Krg	0	0.6117	0.067	0.118
Krw	0	1	0.363	0.323

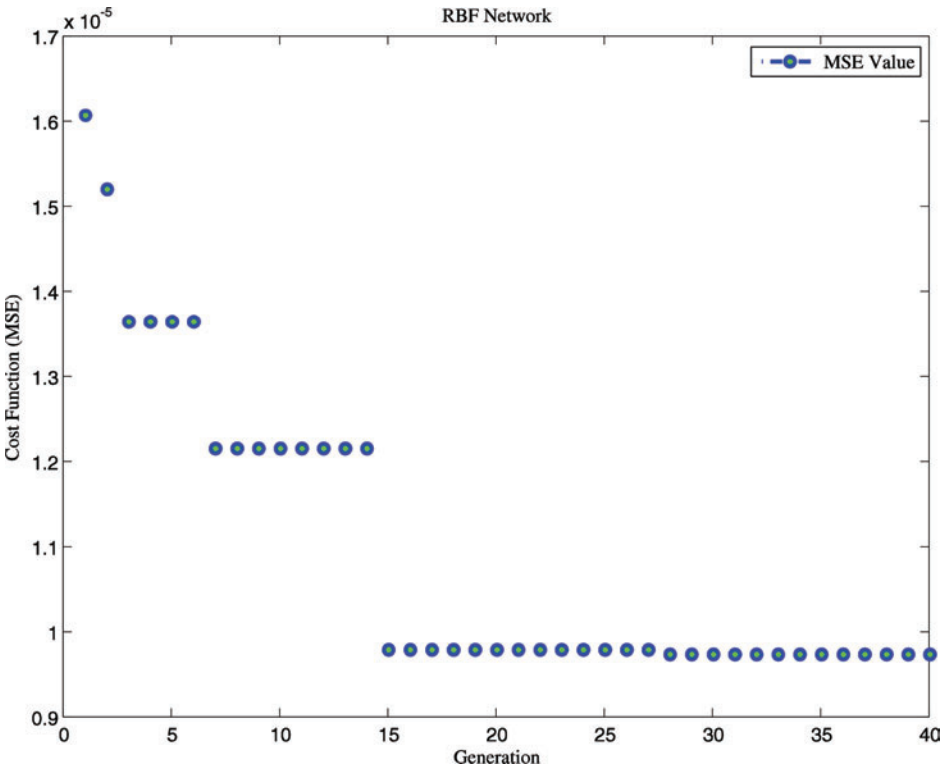

Figure 2. Performance of genetic algorithm in convergence to the optimum values to determine CO_2 relative permeability.

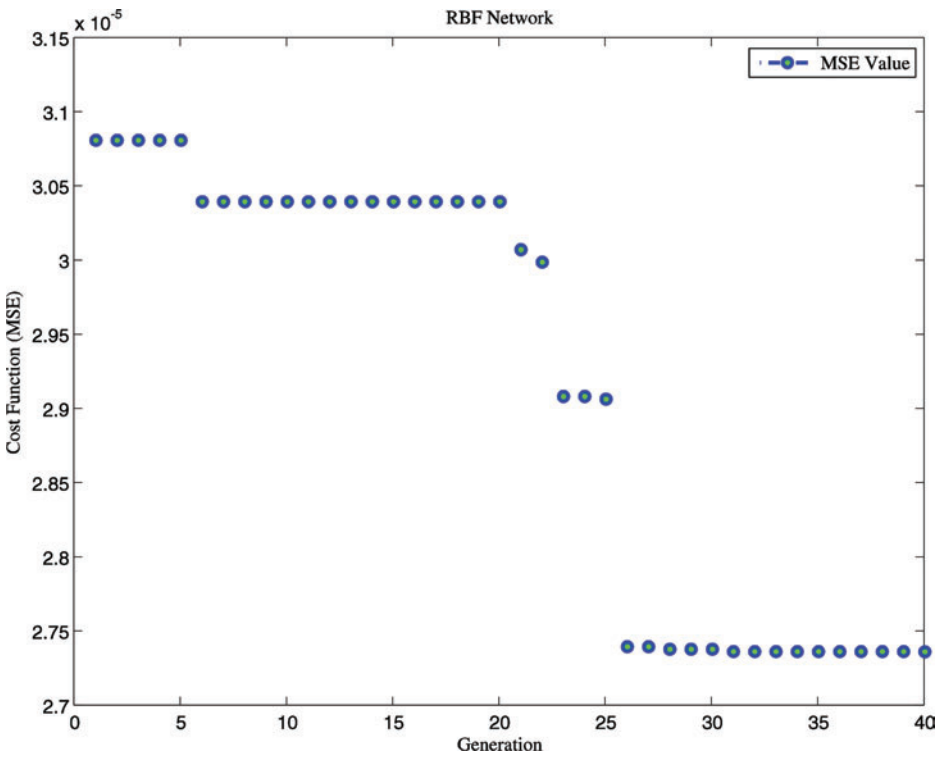

Figure 3. Performance of genetic algorithm in convergence to the optimum values to determine brine relative permeability.

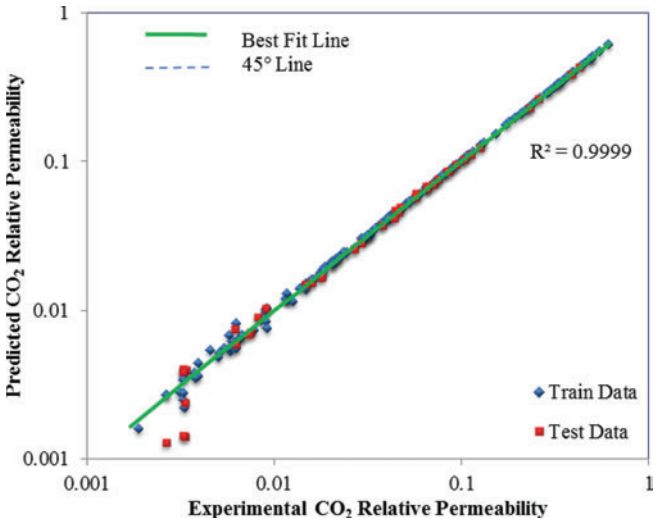

Figure 4. Cross-plot of experimentally observed data points versus GA-RBF predictions for CO_2 relative permeability.

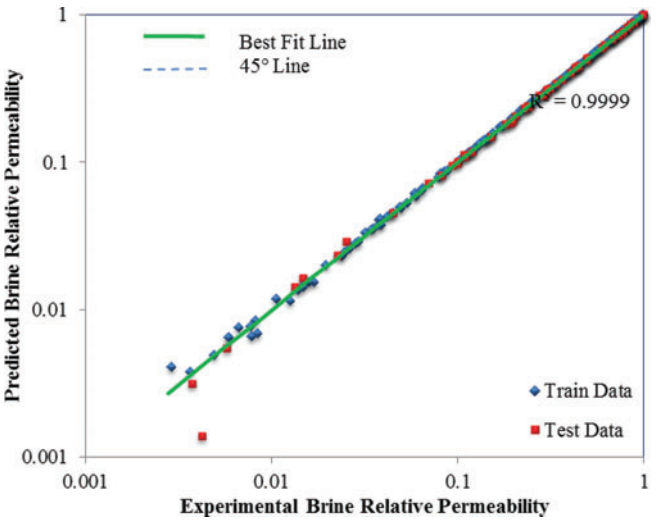

Figure 5. Cross-plot of experimentally observed data points versus GA-vRBF predictions for brine relative permeability.

dard Deviation (STD), and Root Mean Squared Error (RMSE) - have been utilized in order to display the statistical validity of the results (Eqns (11)-(14)). λ reflects the subject parameter, which in this study is relative permeability of CO_2 and brine.

$$R^2 = 1 - \frac{\sum_{i=1}^{N}\left(\lambda_{Pred}(i) - \lambda_{Exp}(i)\right)^2}{\sum_{i=1}^{N}\left(\lambda_{Pred}(i) = \overline{\lambda}_{Exp}\right)^2} \tag{11}$$

$$\%AARD = \frac{100}{N}\sum_{i=1}^{N}\frac{\left(\lambda_{Pred}(i) - \lambda_{Exp}(i)\right)}{\lambda_{Exp}(i)} \tag{12}$$

$$RMSE = \left(\frac{\sum_{i=1}^{N}\left(\lambda_{Pred}(i) - \lambda_{Exp}(i)\right)^2}{N}\right)^{0.5} \tag{13}$$

$$STD = \sum_{i=1}^{N}\left(\frac{\left(\lambda_{Pred}(i) - \overline{\lambda}_{Exp}(i)\right)^2}{N}\right)^{0.5} \tag{14}$$

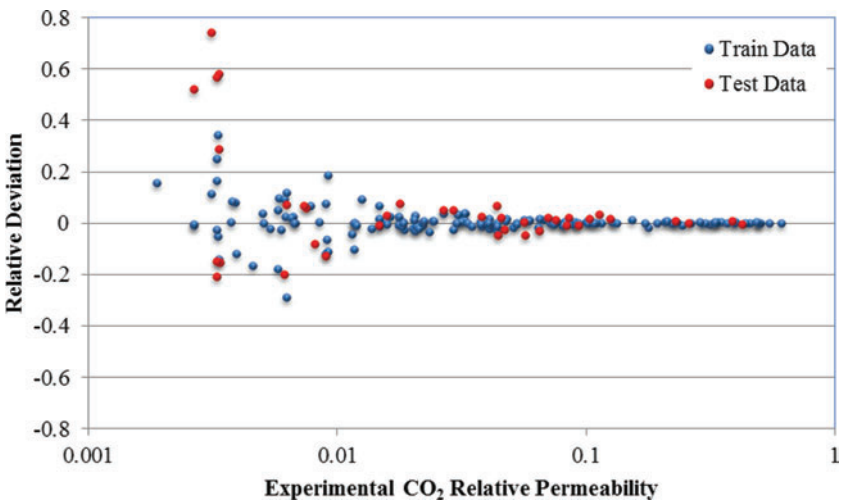

Figure 6. Relative deviation of GA-RBF predictions from experimentally measured values for CO_2 relative permeability.

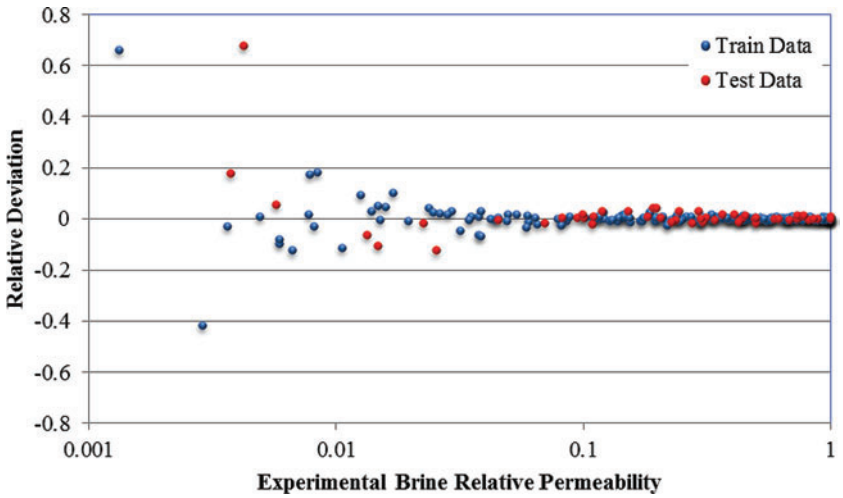

Figure 7. Relative deviation of GA-RBF predictions from experimentally measured values for brine relative permeability.

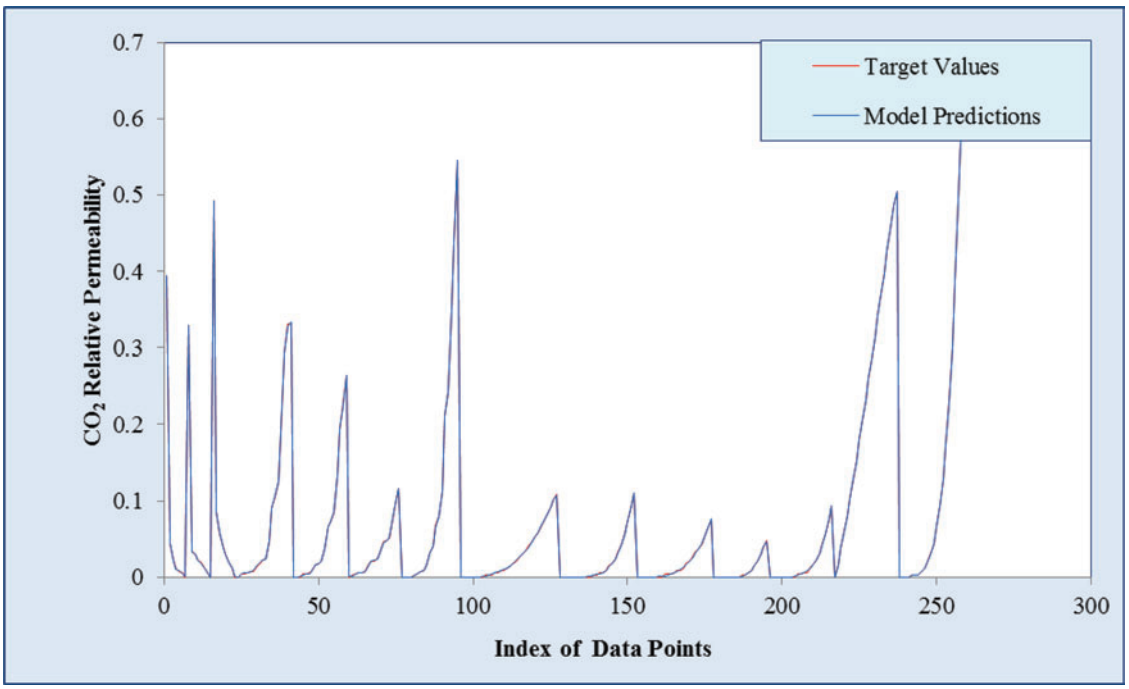

Figure 8. Simultaneous representation of GA-RBF predicted and real values for CO_2 relative permeability.

These parameters represent the applicability and accuracy of the proposed model. Overall values of 0.99993, 4.66171, 0.10899, and 0.00095 for CO_2 relative permeability and 0.99993, 2.10291, 0.07308, and 0.00265 for brine relative permeability for R^2, AARD, STD, and RMSE, respectively, show that the proposed GA-RBF models are suitable for the accurate prediction of supercritical CO_2/brine relative permeability. Details of these parameters for all data sets (testing, training, and total) are presented in Table 3 for both CO_2 and brine models.

The proposed model has been compared with Corey correlation[55] and by power laws[56] models, which are used as numerical and mathematical reservoir simulators.[33] Corey correlation[55] may be utilized alongside CO_2 and brine saturation and irreducible water saturation in order to determine relative permeability. For gas/water systems, Corey correlation can be stated as follows:

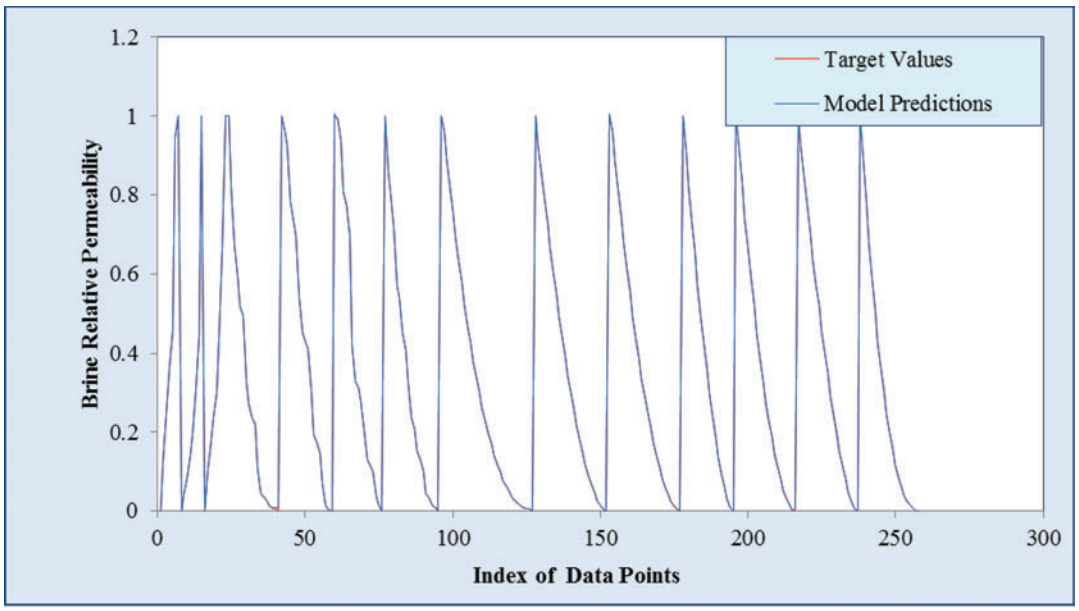

Figure 9. Simultaneous representation of GA-RBF predicted and real values for Brine relative permeability.

Table 3. Statistical parameters for GA-RBF model for CO_2 and brine relative permeability predictions.

		R^2	AARD	STD	RMSE	N
CO_2 Relative Permeability	Train Data	0.99997	2.97287	0.06203	0.00071	206
	Test Data	0.99964	11.45457	0.20668	0.00157	52
	All Data	0.99993	4.66171	0.10899	0.00095	258
Brine Relative Permeability	Train Data	0.99996	1.77382	0.06310	0.00212	206
	Test Data	0.99981	3.37979	0.10320	0.00409	52
	All Data	0.99993	2.10291	0.07308	0.00265	258

Table 4. Power-laws exponents for different datasets utilized in this study.[33]

Source	Area	*n*	*m*
Krevor et al.[34]	Area #1	2.6	3.2
	Area #2	3.0	4.6
	Area #3	1.6	6
Bennion and Bachu[53]	Area #4	3.2	2.9
	Area #5	2.8	1.7
	Area #6	2.2	2.1
	Area #7	5.0	1.8
Bennion and Bachu[54]	Area #8	2.9	2.3
	Area #9	5.2	1.7
	Area #10	3.7	1.8
	Area #11	4.8	1.6
	Area #12	5.6	1.4
	Area #13	5.4	1.8
	Area #14	1.2	1.6

$$k_{rg} = \left(\frac{S_g}{1-S_{iw}}\right)^2 \left(1-\left(\frac{1-S_g-S_{iw}}{1-S_{iw}}\right)^2\right) \quad (15)$$

$$k_{rw} = \left(\frac{S_w-S_{iw}}{1-S_{iw}}\right)^4 \quad (16)$$

where k_{rg} is CO_2 relative permeability, k_{rw} is brine relative permeability, S_g is gas saturation, S_w is brine relative permeability, and S_{iw} is irreducible brine saturation.

Power laws can be presented as follows:

$$k_{rg} = k_{rg0}\left(\frac{S_g-S_{gc}}{1-S_{gc}-S_{iw}}\right)^n \quad (17)$$

$$k_{rw} = k_{rw0}\left(\frac{1-S_g-S_{iw}}{1-S_{gc}-S_{iw}}\right)^m \quad (18)$$

Table 5. Comparison of statistical parameters for different predictive models of CO_2 relative permeability.

		Corey			Power Low Model			GA-RBF Model		
Area	N	R^2	AARD	RMSE	R^2	AARD	RMSE	R^2	AARD	RMSE
Area #1[34]	7	0.996223	128.6788	0.252443	0.998195	39.72527	0.006176	1.00000	0.080942	8.66E-06
Area #2[34]	8	0.981982	225.2962	0.26702	0.995302	44.7095	0.008255	1.00000	0.077292	1.83E-05
Area #3[34]	8	0.985455	70.02175	0.192953	0.998492	18.4372	0.00682	0.999947	0.974771	0.001209
Area #4[53]	18	0.990776	202.0813	0.323274	0.997961	37.47559	0.010008	0.999956	3.049027	0.000791
Area #5[53]	18	0.992386	303.4992	0.347596	0.999762	13.82594	0.001589	0.999978	2.165494	0.000419
Area #6[53]	17	0.995836	438.3587	0.354657	0.997005	33.44767	0.003928	0.999803	3.796434	0.000498
Area #7[53]	19	0.893233	553.6462	0.336752	0.997971	20.40934	0.012996	0.99994	1.663418	0.001338
Area #8[54]	32	0.98877	1099.329	0.463043	0.999436	6.90814	0.000913	0.999464	6.959868	0.000832
Area #9[54]	25	0.878953	2594.681	0.544535	0.999315	7.846404	0.000995	0.999449	7.315358	0.000884
Area #10[54]	25	0.962679	2195.848	0.513451	0.998235	10.06959	0.001164	0.998378	11.01802	0.00112
Area #11[54]	18	0.906437	4648.207	0.624695	0.997727	9.297359	0.000835	0.997832	11.67292	0.00099
Area #12[54]	21	0.894083	2723.328	0.547845	0.996614	18.78537	0.002947	0.998992	8.25763	0.00116
Area #13[54]	21	0.919694	56.82159	0.192415	0.999256	6.296094	0.011504	0.999943	0.565996	0.001228
Area #14[54]	21	0.923271	475.3296	0.272882	0.999854	13.01849	0.003528	0.99991	4.115652	0.001015
total	258	0.950698	1122.509	0.373826	0.998223	20.018	0.005118	0.999542	4.408059	0.000822

Table 6. Comparison of statistical parameters for different predictive models of brine relative permeability.

		Corey			Power Low Model			GA-RBF Model		
Area	N	R^2	AARD	RMSE	R^2	AARD	RMSE	R^2	AARD	RMSE
Area #1[34]	7	0.97173	16.39910	0.07158	0.96100	13.03166	0.08086	1.00000	0.00007	4.E-07
Area #2[34]	8	0.92010	27.57671	0.12589	0.93372	19.67003	0.10545	1.00000	0.00002	5.E-08
Area #3[34]	8	0.95581	53.59246	0.13585	0.99035	7.23920	0.03945	0.99998	0.56547	0.00162
Area #4[53]	18	0.98482	45.21523	0.07039	0.99858	19.78066	0.01271	0.99988	2.91375	0.00305
Area #5[53]	18	0.89721	58.98519	0.19303	0.99987	9.10580	0.00891	0.99996	4.43858	0.00205
Area #6[53]	17	0.94659	55.89091	0.15458	0.99963	8.57064	0.01589	0.99995	1.46031	0.00247
Area #7[53]	19	0.89265	68.19687	0.18368	0.99988	10.63507	0.00602	0.99996	1.01218	0.00214
Area #8[54]	32	0.94409	61.65788	0.12932	0.99992	13.28308	0.00653	0.99995	1.33853	0.00223
Area #9[54]	25	0.88664	67.34159	0.19488	0.99984	5.18100	0.00624	0.99994	2.55590	0.00248
Area #10[54]	25	0.90102	65.20674	0.18128	0.99992	1.97108	0.00372	0.99995	2.04712	0.00240
Area #11[54]	18	0.86081	68.49191	0.21915	0.99983	4.35975	0.00699	0.99992	1.99547	0.00301
Area #12[54]	21	0.90120	66.03096	0.18156	0.99963	3.25199	0.00690	0.99993	1.32551	0.00269
Area #13[54]	21	0.85876	68.30727	0.22181	0.99957	5.79135	0.00904	0.99987	1.52424	0.00394
Area #14[54]	21	0.94999	59.91891	0.11945	0.99984	8.77721	0.00601	0.99989	4.98462	0.00341
total	258	0.91939	55.91512	0.15589	0.99154	9.33204	0.02248	0.99994	1.86870	0.00225

where k_{rg} and k_{rw} are CO_2 and brine relative permeabilities, S_g is CO_2 saturation, S_{gc} is critical CO_2 saturation, k_{rg0}, k_{rw0}, n, and m are the endpoint relative permeabilities and power-law exponents for the brine and CO_2 phases, respectively.

In experimental data utilized in this study, all the authors have assumed $k_{rw0} = 0$ and $S_{gc} = 0$. According to Mathias *et al.*,[33] this assumption has negligible effect on soundness of fit with experimental data. These authors also determined power-laws exponents

for the different data sets used in this study, by least squares fitting to the experimental data. The corresponding values are listed in Table 4. The proposed GA-RBF model was compared with the previously mentioned correlations. Tables 5 and 6 show the statistical parameters for predictive models of CO_2 and brine relative permeability, respectively. The proposed intelligent GA-RBF model may be applied for a more accurate prediction of both CO_2 and brine relative permeability. The AARD for Corey and power-law, and proposed GA-RBF model are presented in Table 5 and 6 for CO_2 and brine, respectively.

Classic methods (simple correlations) have a deficiency in that the effects of effective parameters, such as pressure, temperature, salinity, capillary pressure, interfacial tension and rock type are not included. A further advantage of the proposed GA-RBF is the fact that it is not necessary to determine empirical constants for each data set. Although power laws result in relatively good predictions, it is necessary to determine an empirical constant through curve fitting for each case. In other words, the power law method is case sensitive and is not a general method.

Conclusion

Accurate determination of CO_2/brine relative permeability is of great importance to the simulation and modeling of CO_2/brine system behavior. The objective of this study was to develop a more accurate determination of CO_2/brine relative permeability using a hybrid genetic algorithm-RBF neural network. Excellent agreement between experimental data and predicted values by the proposed GA-RBF model was observed, yielding average absolute relative deviations (AARD) of 4.64 and 2.22% for supercritical CO_2 and brine relative permeability, respectively. A comprehensive comparison between classic correlations and the proposed GA-RBF model has confirmed the superiority of the proposed model. The results obtained from this model demonstrate its suitability for the accurate prediction of CO_2/brine relative permeability.

Appendix A

A Matlab® (Version 2014) program is provided to use the developed model in this study. First of all, download the supplementary file and change the Matlab® directory to the downloaded folder. To get the response from this program follow the instruction step by step.

1. Open the **Sample.xlsx** file. There are two sheets namely **Input** and **Output**. Open the **Input** sheet and feel the determined cells. You can enter more than one data sample. Close the Excel file.
2. Open the **Sample.m** and run. As it is will be prompted by Matlab® for CO_2 Relative permeability enter **1**, otherwise, for brine relative permeability enter **2** and press **Enter**.
3. Open the **Sample.xlsx** and turn to **Output** sheet. The results are provided in their corresponding columns.

To better understand the instruction of using the developed GA-RBF model, the following example has been provided:

Example:
Calculate the CO_2 relative permeability with the data provided in Table A1.

Solution

Because the **Rock Type** input is string and we cannot use the string as an input the following indices have been considered for the following rock types:

Sandstone: 1, Carbonate: 2

First open the **Sample.xlsx** file that has been provided in the **network** folder and fill the input parameters. After that, the following commands must be entered in the MATLAB (version 2014a) command window:

```
clc;
clear;
close all;
type = input('For CO2 Relative Perme-
ability Enter 1, for Brine Relative
Permeability Enter 2: ');
if type = = 1
    %% DATA LOADING
    load CO2
    clear X
    clear XN
    clear InputNum
    clear ii
    clear YtotalNetRBF
    clear RYtotalNetRBF

    X = xlsread('Sample.xlsx');
```


Table A1. The sample set for calculation of CO_2 relative permeability.

Porosity (%)	Permeability (mD)	IFT (mN/m)	Salinity (mg/L)	Pressure (MPa)	Threshold Capillary Pressure (kPa)	Temperature (°C)	Rock Type	Sg	Sw
22.1	914	32	50	9	2.5	50	Sandstone	0.5562	0.4438

```
MinX = [9.900000000000000,0.081000000000
0000,27,50,8.600000000000000,2.1000000000
0000,35,1,0,0.210800000000000];

MaxX = [28.300000000000001156,45.3000000
0000003208472780275,2,0.789200000000000,1];
   MinY = 0;
   MaxY = 0.6117;

   %% Normalization
   XN = X;
   InputNum = size(X,2);
   for ii = 1:InputNum
      XN(:,ii) = Normalize _ Fcn(X(:,ii)
     ,MinX(ii),MaxX(ii));
 end

   %% Assessment

   YtotalNetRBF = sim(Network,XN')';
   RYtotalNetRBF =
 Realize _ Fcn(YtotalNetRBF,MinY,MaxY);

   %% Export to Excel
   xlswrite('Sample.xlsx',RYtotalNetRBF
 ,'Output','K3');
 else

 %% DATA LOADING
    load Brine
    clear X
    clear XN
    clear InputNum
    clear ii
    clear YtotalNetRBF
    clear RYtotalNetRBF

 X = xlsread('Sample.xlsx');

MinX = [9.900000000000000,0.081000000000
0000,27,50,8.600000000000000,2.1000000000
0000,35,1,0,0.210800000000000];

MaxX = [28.300000000000001156,45.30000
000000003208472780275,2,0.7892000000000
00,1];
  MinY = 0;
  MaxY = 1;
  %% Normalization
  XN = X;
  InputNum = size(X,2);
  for ii = 1:InputNum
      XN(:,ii) = Normalize _ Fcn(X(:,ii)
   ,MinX(ii),MaxX(ii));
  end

  %% Assessment

  YtotalNetRBF = sim(Network,XN')';
  RYtotalNetRBF =
 Realize _ Fcn(YtotalNetRBF,MinY,MaxY);

  %% Export to Excel
  xlswrite('Sample.xlsx',RYtotalNetRBF
 ,'Output','K3');
 end
```

To simplify running the model, instead of typing the above commands in command window, please run the **Run.m** to calculate the relative CO_2 relative permeability. After reuning the program, please input "1" to calculate CO_2 relative permeability.

The result is 0.394804087, where its experimental value is equal to 0.3948 (the relative deviation is 1.03%).

References

1. Metz B, Change I. P. o. C.; III., I. P. o. C. C. W. G., Climate Change 2007. In *Mitigation of Climate Change, Contribution of Working Group III to the Fourth Assessment Report of the IPCC*, Cambridge University Press: 2007; p 851.
2. Benson SM and Cole DR, CO_2 Sequestration in deep sedimentary formations. *Elements* **4**(5):325–331 (2008).
3. Bajura RA, The role of carbon sequestration in the longer term energy future. *International Conference on Greenhouse Gas Control Technologies: GHGT-5*, Cairns, Queensland, Australia, 13–16CSIRO Publishing, Collingwood, Victoria, Australia (2001).

4. Gielen D, Podkański J, Agency IE, Development, O. E. C., *Prospects for CO_2 Capture and Storage*. OECD/IEA: 2004.
5. Benson S and Cook P, Underground geological storage. In *IPCC Special Report on Carbon Dioxide Capture and Storage*. Ed by B., M.; O., D.; H.C., d. C.; M., L.; L.A., M., Cambridge University Press, pp 195–276 (2005).
6. Bachu S, Bonijoly D, Bradshaw J, Burruss R, Holloway S, Christensen NP, and Mathiassen OM, CO_2 storage capacity estimation: Methodology and gaps. *Int J Greenhouse Gas Control* **1**(4): 430–443 (2007).
7. Gale J, Geological storage of CO_2: What do we know, where are the gaps and what more needs to be done?*Energy* **29**(9–10):1329–1338 (2004).
8. Bennion B and Bachu S, Relative Permeability Characteristics for Supercritical CO_2 Displacing Water in a Variety of Potential Sequestration Zones, *SPE Annual Technical Conference and Exhibition*, Dallas, TX USA, October 9–12 (2005).
9. Bennion DB and Bachu S, The Impact of Interfacial Tension and Pore Size Distribution/Capillary Pressure Character on CO2 Relative Permeability at Reservoir Conditions in CO2-Brine Systems, *SPE/DOE Symposium on Improved Oil Recovery*, Tulsa, OK, USA, April 22–26. pp 1–10 (2006).
10. Brasier F and Kobelski B, Injection of industrial wastes in the United States. In *Deep injection of Disposal of Hazardous Industrial Waste. Scientific and Engineering Aspects*. Ed by Apps JA and Tsang C-F. Academic Press: San Diego, CA, pp 1–8 (1996).
11. Bachu S and Haug K, In-situ characteristics of acid-gas injection operations in the Alberta basin, western Canada. In *Geologic Storage of Carbon Dioxide with Monitoring and Verification*. Ed by Benson SM. Elsevier: London, UK **2**:867–876 (2005).
12. Oldenburg C, Migration mechanisms and potential impacts of CO_2 leakage and seepage. In *Carbon Capture and Sequestration: Integrating Technology, Monitoring, Regulation*. Ed by Wilson, E and Gerard D. Blackwell Publishing: United States, pp 127–146 (2007).
13. Bachu S, Screening and ranking of sedimentary basins for sequestration of CO_2 in geological media in response to climate change. *Environ Geol* **44**(3):277–289 (2003).
14. Gunter WD, Bachu S and Benson S, The role of hydrogeological and geochemical trapping in sedimentary basins for secure geological storage of carbon dioxide. *Geological Society, London, Special Publications* **233**(1):129–145 (2004).
15. Kumar A, Noh MH, Pope GA, Sepehrnoori K, Bryant SL and Lake LW, Simulating CO_2 Storage in Deep Saline Aquifers. In *Carbon Dioxide Capture for Storage in Deep Geologic Formations*, Ed by Thomas DC. Elsevier Science: Amsterdam, pp 877–896 (2005).
16. Ennis-King J and Paterson L, Role of convective mixing in the long-term storage of carbon dioxide in deep saline formations. *SPE Annual Technical Conference and Exhibition*, Society of Petroleum Engineers: Denver, Colorado, pp 1–12 (2003).
17. Xu T, Apps JA and Pruess K, Reactive geochemical transport simulation to study mineral trapping for CO_2 disposal in deep arenaceous formations. *J Geophys Res: Solid Earth (1978–2012)* **108**(B2): (2003).
18. Bachu S and Bennion B, Effects of in-situ conditions on relative permeability characteristics of CO_2-brine systems. *Environ Geol* **54**(8):1707–1722 (2008).
19. Doughty C and Pruess K, Modeling supercritical carbon dioxide injection in heterogeneous porous media. *Vadose Zone Journal* **3**(3):837–847 (2004).
20. Flett M, Gurton R and Taggart I, The function of gas-water relative permeability hysteresis in the sequestration of carbon dioxide in saline formations, *SPE Asia Pacific Oil and Gas Conference and Exhibition*, Perth, Australia (2004).
21. Kopp A, Class H and Helmig R, Investigations on CO_2 storage capacity in saline aquifers: Part 1. Dimensional analysis of flow processes and reservoir characteristics. *Int J Greenhouse Gas Control* **3**(3):263–276 (2009).
22. Cinar Y, Neal PR, Allinson WG, Sayers J, Geoengineering and economic assessment of a potential carbon capture and storage site in Southeast Queensland, Australia. *SPE Reservoir Eval Eng* **12**(5):660–670.
23. Burton M, Kumar N and Bryant SL, CO_2 injectivity into brine aquifers: Why relative permeability matters as much as absolute permeability. *Energy Proc* **1**(1):3091–3098 (2009).
24. Burnside NM and Naylor M, Review and implications of relative permeability of CO_2/brine systems and residual trapping of CO_2. *Int J Greenhouse Gas Control* **23**:1–11 (2014).
25. Levine JS, Goldberg DS, Lackner KS, Matter JM, Supp MG and Ramakrishnan TS, Relative Permeability Experiments of Carbon Dioxide Displacing Brine and Their Implications for Carbon Sequestration. *Environmental Science & Technology* **48**(1), 811–818 (2013).
26. Chang C, Zhou Q, Xia L, Li X and Yu Q, Dynamic displacement and non-equilibrium dissolution of supercritical CO_2 in low-permeability sandstone: An experimental study. *Int J Greenhouse Gas Control* **14**:1–14 (2013).
27. Benson SM, Hingerl F, Li B, Pini R, Tchelepi H and Zuo L, *Investigations in Geologic Carbon Sequestration: Multiphase Flow of CO_2 and Water in Reservoir Rocks*; Stanford University, School of Earth Sciences, Department of Energy Resources Engineering, pp 1–18 (2013).
28. Bachu S, Drainage and imbibition CO_2/brine relative permeability curves at in situ conditions for sandstone formations in western Canada. *Energy Proc* **37**: 4428–4436 (2013).
29. Akbarabadi M and Piri M, Relative permeability hysteresis and capillary trapping characteristics of supercritical CO_2/brine systems: An experimental study at reservoir conditions. *Adv Water Resour* **52**:190–206 (2013).
30. Pini R, Krevor SCM and Benson SM, Capillary pressure and heterogeneity for the CO_2/water system in sandstone rocks at reservoir conditions. *Adv Water Resour* **38**:48–59 (2012).
31. Busch A and Müller N, Determining CO_2 /brine relative permeability and capillary threshold pressures for reservoir rocks and caprocks: Recommendations for development of standard laboratory protocols. *Energy Proc* **4**:6053–6060 (2011).
32. Akbarabadi M and Piri M, Geologic storage of carbon dioxide: an experimental study of permanent capillary trapping and relative permeability. *Proc Soc Core Analysts*Austin, TX, USA18–21 (2011).
33. Mathias SA, Gluyas JG, González Martínez de Miguel GJ, Bryant SL and Wilson D, On relative permeability data uncertainty and CO_2 injectivity estimation for brine aquifers. *Int J Greenhouse Gas Control* **12**:200–212 (2013).
34. Krevor SCM, Pini R, Zuo L and Benson SM, Relative permeability and trapping of CO_2 and water in sandstone rocks at reservoir conditions. *Water Resour Res* **48**(2):W02532 (2012).

35. Bennion DB and Bachu S, Dependence on Temperature, Pressure, and Salinity of the IFT and Relative Permeability Displacement Characteristics of CO_2 Injected in Deep Saline Aquifers, *SPE Annual Technical Conference and Exhibition*, San Antonio, TX, USA, September 24–27. Society of Petroleum Engineers: San Antonio, TX, USA (2006).
36. Müller N, Supercritical CO_2-brine relative permeability experiments in reservoir rocks—literature review and recommendations. *Transport Porous Med* **87**(2):367–383 (2011).
37. Tatar A, Yassin MR, Rezaee M, Aghajafari AH and Shokrollahi A, Applying a robust solution based on expert systems and GA evolutionary algorithm for prognosticating residual gas saturation in water drive gas reservoirs. *J Nat Gas Sci Eng* **21**:79–94 (2014).
38. Tatar A, Shokrollahi A, Halali MA, Azari V and Safari H, A hybrid intelligent computational scheme for determination of refractive index of crude oil using SARA fraction analysis. *Can J Chem Eng* (2015).
39. Nouri-Taleghani M, Mahmoudifar M, Shokrollahi A, Tatar A and Karimi-Khaledi M, Fracture density determination using a novel hybrid computational scheme: a case study on an Iranian Marun oil field reservoir. *J Geophys Eng* **12**(2):188 (2015).
40. Shokrollahi A, Tatar A and Safari H, On accurate determination of PVT properties in crude oil systems: Committee machine intelligent system modeling approach. *J Taiwan Inst Chem Eng* (0).
41. Santos RB, Ruppb M, Bonzi SJ and Filetia AMF, Comparison between multilayer feedforward neural networks and a radial basis function network to detect and locate leaks in pipelines transporting gas. *Chem Eng Trans* **32**:1375–1380 (2013).
42. Hao Y, Tiantian X, Paszczynski S and Wilamowski BM, Advantages of radial basis function networks for dynamic system design. *Industrial Electronics, IEEE Transactions on* **58**(12):5438–5450 (2011).
43. Du K-L and Swamy MNS, Radial Basis Function Networks. In *Neural Networks in a Softcomputing Framework*, Springer, London, pp 251–294 (2006).
44. Powell MJD, Radial basis functions for multivariable interpolation: a review. In *Algorithms for Approximation*. Ed by Mason JC and Cox MG . Clarendon Press, London, pp 143–167 (1987).
45. Wilamowski BM and Jaeger RC, Implementation of RBF Type Networks by MLP Networks, *Neural Networks, IEEE International Conference* June 3–6 **3**:1670–1675 (1996).
46. Poggio T and Girosi F, Networks for approximation and learning. *Proc. IEEE* **78**(9):1481–1497 (1990).
47. Girosi F and Poggio T, Networks and the best approximation property. *Biological Cybernetics* **63**(3):169–176 (1990).
48. Liao Y, Fang S-C and Nuttle HLW, Relaxed conditions for radial-basis function networks to be universal approximators. *Neural Networks* **16**(7):1019–1028 (2003).
49. Shan O and Zheng B, Fast principal component extraction by a weighted information criterion. *Signal Processing, IEEE Transactions on* **50**(8):1994–2002 (2002).
50. Park J and Sandberg IW, Universal approximation using radial-basis-function networks. *Neural Computation* **3**(2): 246–257 (1991).
51. Devijver PA and Kittler J, *Pattern Recognition: A Statistical Approach*. Prentice/Hall International: Englewood Cliffs , NJ, 1982.
52. Micchelli C, Interpolation of scattered data: distance matrices and conditionally positive definite functions. In *Approximation Theory and Spline Functions*. Ed by Singh SP, Burry JWH , Watson B. Springer, Netherlands. **136**:143–145 (1984).
53. Bennion B and Bachu S, Drainage and imbibition relative permeability relationships for supercritical CO_2/brine and H_2S/brine systems in intergranular sandstone, carbonate, shale, and anhydrite rocks. *SPE Reservoir Evaluation & Engineering* **11**(3):487–496 (2008).
54. Bennion B and Bachu S, Drainage and imbibition CO_2/Brine relative permeability curves at reservoir conditions for high-permeability carbonate rocks. *SPE Annual Technical Conference and Exhibition*, Society of Petroleum Engineers, Florence , Italy, pp 1–18 (2010).
55. Corey AT, The interrelation between gas and oil relative permeabilities. *Producers Monthly* **19**(1):38–41 (1954).
56. Orr FM, *Theory of Gas Injection Processes*. Tie-Line Publications (2007).

Afshin Tatar

Afshin Tatar is a member of the Young Researchers and Elite Club, North Tehran Branch, at the Islamic Azad University, Tehran, Iran. He is a graduate student of petroleum reservoir engineering from the Petroleum University of Technology in Ahwaz, Iran. His current research interests include reservoir simulation, fluid flow assurance, asphaltene deposition, and ionic liquids.

Amin Shokrollahi

Amin Shokrollahi received his BSc from the Petroleum University of Technology and an MSc degree in Petroleum Reservoir Engineering from Sharif University of Technology, Tehran, Iran. His current research interests include EOR methods, fluid flow in porous media, and reservoir simulation and modeling.

Tomoaki Kashiwao

Tomoaki Kashiwao has been an Assistant Professor at the National Institute of Technology, Niihama College, Japan since 2010 and a Visiting Fellow at Southern Cross University, Australia since 2015. He received his Dr Eng. from Tokushima University, Japan in 2009. His research interests include hybrid systems, LED packaging, and neural networks.

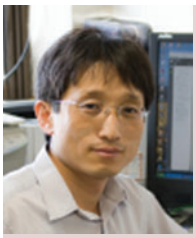

Moonyong Lee

Moonyong Lee has been a professor in Yeungnam University since 1994. His research interests include modeling and design of chemical processes. He received his BSc, MSc and PhD in Chemical Engineering from Seoul National University in 1982, and KAIST in 1984 and 1991, respectively. From 1984 to 1994, he worked in SK refinery and petrochemical plant.

Alireza Bahadori

Alireza Bahadori, PhD, PEng, is a lecturer with the School of Environment, Science and Engineering at Southern Cross University, Lismore, NSW, Australia. He received his PhD from Curtin University, Perth, WA, Australia. He is the author of several books published by multiple major publishers, including Elsevier, Springer and John Wiley & Sons.